

# Solar cycle related changes at the base of the convection zone

Charles S. Baldner and Sarbani Basu

*Department of Astronomy, Yale University, P.O. Box 208101, New Haven, CT, 06520-8101*

charles.baldner@yale.edu

## ABSTRACT

The frequencies of solar oscillations are known to change with solar activity. We use Principal Component Analysis to examine these changes with high precision. In addition to the well-documented changes in solar normal mode oscillations with activity as a function of frequency, which originate in the surface layers of the Sun, we find a small but statistically significant change in frequencies with an origin at and below the base of the convection zone. We find that at  $r = (0.712^{+0.0097}_{-0.0029})R_{\odot}$ , the change in sound speed is  $\delta c^2/c^2 = (7.23 \pm 2.08) \times 10^{-5}$  between high and low activity. This change is very tightly correlated with solar activity. In addition, we use the splitting coefficients to examine the latitudinal structure of these changes. We find changes in sound speed correlated with surface activity for  $r \gtrsim 0.9R_{\odot}$ .

*Subject headings:* Sun: helioseismology, Sun: activity, Sun: interior

## 1. INTRODUCTION

Normal modes of oscillation of the Sun have provided a powerful tool to peer into the solar interior. In particular, modern experiments, both ground- and space-based, have measured the intermediate degree global oscillation spectrum with high precision since the beginning of solar cycle 23. Accurate determinations of interior structure and dynamics are now possible (see, e.g., review by Christensen-Dalsgaard 2002). These measurements contain a wealth of information about the fundamental causes of solar variability.

It is generally believed that the seat of the solar dynamo is located at the base of the convection zone (e.g., review by Charbonneau 2005). Because helioseismology provides the only direct measurements of this region of the solar interior, these results can play an important role in constraining dynamo theories. In particular, a number of authors have attempted to use global and local helioseismic techniques to determine limits on the strength

of the magnetic field at the base of the convection zone (e.g., Chou et al. 2003, and references therein). In this paper, we attempt to improve helioseismic measurements of changes in this region.

Global modes of solar oscillation are described by three numbers that characterize the spherical harmonics that are used to define the horizontal structure of the mode. These are (1) radial order  $n$  that related to the number of nodes in the radial direction, (2) the degree  $\ell$  that is related to the horizontal wavelength of the mode, and (3) the azimuthal order  $m$  that defines the number of nodes along the equator. In a spherically symmetric star, the  $2\ell + 1$  modes of an  $(n, \ell)$  multiplet are degenerate, but effects that break spherical symmetry such as magnetic fields or rotation lift the degeneracy and results in frequency splittings. The frequencies  $\nu_{n\ell m}$  of the modes within a multiplet can be expressed as an expansion in orthogonal polynomials:

$$\nu_{n\ell m} = \nu_{n\ell} + \sum_{j=1}^{j_{\max}} a_j(n, \ell) \mathcal{P}_j^{(\ell)}(m). \quad (1)$$

Early investigators (e.g., Duvall et al. 1986) commonly used Legendre polynomials, whereas now one often uses the Ritzwoller-Lavelly formulation of the Clebsch-Gordan expansion (Ritzwoller & Lavelly 1991) where the basis functions are polynomials related to the Clebsch-Gordan coefficients. In either case, the coefficients  $a_j$  are referred to as  $a$ -coefficients or splitting coefficients. Solar structure is determined by inverting the mean frequency  $\nu_{n\ell}$ , while the odd-order coefficients  $a_1, a_3, \dots$  depend principally on the rotation rate (Durney et al. 1988) and reflect the advective, latitudinally symmetric part of the perturbations caused by rotation. Hence, these are used to determine the rate of rotation inside the Sun. The even order  $a$  coefficients on the other hand result from magnetic fields and asphericities in solar structure, and the second order effects of rotation (e.g., Gough & Thompson 1990; Dziembowski & Goode 1991).

Solar oscillation frequencies are known to vary on timescales related to the solar activity cycle. This was first suggested by Woodard & Noyes (1985) and confirmed soon after by Elsworth et al. (1990) and Libbrecht & Woodard (1990). It was quickly established that the frequency shifts were strongly correlated with surface activity (Woodard et al. 1991; Bachmann & Brown 1993; Elsworth et al. 1994; Regulo et al. 1994, etc.). Libbrecht & Woodard (1990) observed that the frequency shifts depended very strongly on mode frequency  $\nu$ , and very weakly on degree  $\ell$  of the mode, and Anguera Gubau et al. (1992) and Elsworth et al. (1994) confirmed these results. These authors concluded that all or most of the physical changes responsible for the changes in frequency were confined to the shallow layers of the Sun. In general, this picture has been confirmed in more recent studies (e.g., observational results: Howe et al. 1999, 2002; Basu & Antia 2000; Verner et al. 2004; Dziembowski & Goode

2005, etc., and theoretical results: Goldreich et al. 1991; Balmforth et al. 1996; Li et al. 2003, etc.). A change in the second helium ionization zone at  $r = 0.98R_{\odot}$ , first suggested by Goldreich et al. (1991) and Gough (2002), has been confirmed by Basu & Mandel (2004) and Verner et al. (2006).

The even-order mode splitting parameters sample effects of structural asphericities on the mode frequency. Kuhn (1988) suggested that they were correlated with observed changes in surface temperature. Subsequent work has shown that the aspherical components of the mode frequencies are tightly correlated with surface magnetic activity (Howe et al. 1999; Antia et al. 2001). This high correlation lends further credence to the idea that frequency shifts are caused by surface and/or near-surface effects. This can be tested directly with high degree modes that sample the near-surface layers of the Sun. However, as the degree  $l$  increases, global modes become increasingly hard to measure precisely due to the decrease in mode lifetimes (Rhodes et al. 1998; Rabello-Soares et al. 2001; Korzennik et al. 2004). The lack of reliable measurements of these modes has led some authors to use ring diagrams to measure high degree modes and measure changes in the shallow layers of the solar convection zone. These studies have confirmed that structural changes do occur in the near-surface layers of the Sun (Basu et al. 2007).

Direct inversions of changes in the structure of the solar interior probed by the spherically symmetric global modes have not yielded any measurable differences in the deep interior (Basu 2002; Eff-Darwich et al. 2002) and there have been upper limits placed on the changes at the base of the convection zone (Eff-Darwich et al. 2002). Chou & Serebryanskiy (2005) and Serebryanskiy & Chou (2005) have presented evidence of a possible change in mode frequencies with lower turning points near the base of the convection zone.

Internal dynamics, on the other hand, show clear and unequivocal evidence of change over the course of the solar cycle. In the convection zone, bands of different rotational velocities (called zonal flows) have been shown to migrate poleward at high latitudes and equator-ward at low latitudes (Schou 1999; Howe et al. 2000; Antia & Basu 2000, 2001). Temporal variations in dynamics have been shown to penetrate throughout the entire convection zone, and even below (Vorontsov et al. 2002; Basu & Antia 2006; Howe et al. 2005, 2006).

One conclusion that can be drawn unequivocally from previous studies of the changes in solar structure is that any changes deeper than those in the outermost layers of the Sun are very small, and hence very difficult to detect through their signatures in oscillation frequencies. Chou & Serebryanskiy (2005) used a smoothing technique to attempt to remove the effect of surface variations, and found that the scaled frequency differences showed evidence of change near the base of the convection zone, but could not say more about the physi-

cal nature of the changes. Attempts to invert the frequencies directly have never shown any changes larger than the inversion errors (e.g., Basu 2002; Eff-Darwich et al. 2002). Therefore, although current helioseismic instruments have determined the solar oscillation frequencies with tremendous precision, statistical errors in those frequencies are still too large to make any direct detections of structure changes in the deep interior.

In this work, we take a somewhat different approach to attempting to detect changes at the base of the convection. We use Principal Component Analysis (PCA) to separate the frequency differences over the last solar cycle into a linear combination of different time-dependent components. This has the effect of decreasing the effects of measurement errors in the measured helioseismic frequencies, which allows us to isolate as precisely as possible the changes in frequency over time. In section 2, we describe the data used, and the methods employed to analyze them. In section 3, we present the results in detail. Finally, in section 4 we discuss the significance of the results and presents our conclusions.

## 2. DATA & ANALYSIS

### 2.1. Data

For this work, we use helioseismic global-mode data sets from two different projects, one from the Michelson Doppler Imager (MDI) on-board the SOHO spacecraft, and the other from the Global Oscillations Network Group (GONG). The MDI mode sets consist of frequencies and splittings obtained from 72-day long time series (Schou 1999). We use 54 of these sets, spanning the period from 1996 May 1 to 2007 May 16. The GONG mode sets are derived from 108-day time series (Hill et al. 1996). Although GONG provides sets that overlap in time, we only use non-overlapping sets in the present work. We use 40 sets from the period 1995 May 7 to 2007 April 14. Because the two sets are from completely different instruments and independent data reduction pipelines, any real solar signatures should show up in both sets. The  $f$ -modes do not sample the deep interior and are dominated by surface effects, so we exclude them from our study. The  $n = 1$  modes have larger errors than the higher order modes, and so we exclude them as well. The included modes are low and intermediate degree modes up to  $\ell = 176$ , with order  $n$  from 2 to 16.

As a proxy for total solar activity, we use the 10.7cm radio flux measurements taken by the Dominion Radio Astrophysical Observatory (DRAO) <sup>1</sup>. This measurement has been

---

<sup>1</sup>Data can be found at [http://www.drao-ofr.hia-ihh.nrc-cnrc.gc.ca/icarus/www/sol\\_home.shtml](http://www.drao-ofr.hia-ihh.nrc-cnrc.gc.ca/icarus/www/sol_home.shtml)

found to be very tightly correlated with solar activity (e.g., Tapping 1987). We average the  $F_{10.7}$  measurements over 72-day periods for comparison with MDI data, and 108-day periods for comparison with GONG data. For latitudinal structure in surface activity, we use the surface magnetic field, taken from SOHO/MDI synoptic maps <sup>2</sup>. The magnetic field strengths are averaged over the same 72-day periods as the  $F_{10.7}$  data, and over the appropriate ranges in latitude.

## 2.2. Method

We use Principal Component Analysis to describe the temporal variations of the weighted frequencies as a small number of uncorrelated basis functions. The use of PCA is a common technique in multivariate data analysis to reduce dimensionality and expose underlying variables (see Murtagh & Heck 1987, Chapter 2, for a discussion of its astrophysical applications). A brief description of the method and discussion of its limitations is included in the Appendix. PCA is a technique whereby a set of observations is expressed as a set of uncorrelated vectors. The usefulness of the technique arises from the fact that variation of the data about the first vector is maximal, and about the second vector, maximal subject to the constraint that it be orthogonal to the first vector, and so on. In other words, PCA provides a very efficient linear representation of a data set, and it is able to substantially reduce the dimensionality of the data set without losing any significant information.

It has been known for many years that the frequencies of the solar global modes of oscillation change with the solar activity cycle. With the arrival of high quality measurements of intermediate degree modes, it is clear that the amount of frequency shift over the solar cycle is dependent on the mode. Each mode has an associated mode inertia  $E_{nl}$ . Frequency differences can be scaled by the quantity  $Q_{nl} = E_{nl}/\bar{E}_0(\nu_{nl})$ , where  $\bar{E}_0(\nu_{nl})$  is the inertia of the  $\ell = 0$  modes interpolated to the frequency of the  $(n, \ell)$  mode (Christensen-Dalsgaard & Berthomieu 1991). This scaling accounts for the fact that the frequencies of modes with lower inertia are changed by a larger amount than modes with a higher inertia by the same underlying perturbation. When scaled in this way, the degree-dependence of the frequencies over the solar cycle largely vanish, and the frequency changes become slowly varying functions of frequency only (e.g., Chaplin et al. 2001; Basu 2002).

Our data points are the scaled frequency differences  $Q_{nl}\delta\nu_{nl}/\nu_{nl}$ . For the MDI observations, there are 54 total mode sets in our work, which, when one is removed to be used

---

<sup>2</sup>MDI synoptic maps of Carrington rotations can be found at <http://soi.stanford.edu/magnetic/index6.html>

as the base set, giving us 53 sets of scaled frequency differences. There are 40 mode sets in our GONG data set, or 39 difference sets. Because the PCA method requires a complete covariance matrix (see the Appendix), we can only include a mode if it is present in all mode sets. This dramatically reduces the amount of usable information, particularly since many excluded modes are missing in only one or two sets out of 53. For these modes, it is possible to interpolate a value for the missing frequency differences. In this case, because most of the frequency differences for the mode in question will be actually observed, any errors introduced through the interpolation will have a negligible effect on the PCA results. We tested two interpolation methods — one a spline interpolation along ridges in the  $\ell$ - $\nu$  diagram (interpolated from modes with the same radial order  $n$ ), and the other a linear interpolation between neighboring modes in time. When tested against existing modes, the interpolation along time proved superior, reproducing the actual data to better than a factor of  $1.2\sigma$ , while the interpolation along the ridge results had a  $2\sigma$  distribution. Therefore, only results using the time interpolation are discussed in this paper, but the PCA results using interpolation over degree were entirely consistent. Finally, to ensure that the PCA is robust, Monte Carlo simulations were performed to ensure that the exclusion of certain modes would not affect the results. The PCA analysis of these data appears to be very robust. Errors in the PCA components were computed by means of a Monte Carlo simulation.

In addition to the mean frequencies  $\nu_{n\ell}$ , which contain information about the spherically symmetric part of the solar interior, we have the even-order splitting coefficients  $a_{2j}(n, \ell)$ , which allow us to reproduce mode frequencies as a function of latitude. Latitudinal frequencies as a function of colatitude  $\theta$  can be obtained as follows:

$$\nu_{n\ell}(\theta) = \nu_{n\ell} + \sum_k \frac{\ell a_{2k}(n, \ell)}{\mathcal{Q}_{\ell k}} P_{2k}(\cos \theta), \quad (2)$$

where  $\mathcal{Q}_{\ell k}$  are the angular integrals given by

$$\int_0^{2\pi} d\phi \int_0^\pi \sin \theta d\theta Y_\ell^m (Y_\ell^m)^* P_{2k}(\cos \theta) = \frac{1}{\ell} \mathcal{Q}_{\ell k} \mathcal{P}_{2k}^{(\ell)}(m), \quad (3)$$

and  $P_{2k}(\cos \theta)$  are Legendre polynomials of degree  $2k$ , and the  $\mathcal{P}_{2k}^{(\ell)}$  are the same polynomials as in equation 1.

Ultimately, we are interested in helioseismic data for what they can tell us about the solar interior. To extract this information, we invert these data sets for the parameters of interest. We use two different inversion techniques, and invert for the change in sound speed relative to the comparison frequency. The first technique used is Subtractively Optimized Local Averages (SOLA Pijpers & Thompson 1994). A description of the implementation used here, and how to select inversion parameters can be found in Rabello-Soares et al. (1999). The

second inversion technique is that of Regularized Least Squares (RLS). The implementation used here and the selection of inversion parameters have been discussed in Antia & Basu (1994) and Basu & Thompson (1996). The use of these two techniques in tandem is crucial because the techniques are complimentary in nature (Sekii 1997). Inversions can be trusted if both inversion techniques return the same results.

The quantities which we invert are appropriately scaled eigenvectors from the PCA of the frequency differences. The differences are taken relative to some fiducial set, usually the first mode set (corresponding to activity minimum at the beginning of solar cycle 23). The eigenvectors,  $\xi_i$ , are normalized so that  $\xi_i \cdot \xi_i = 1$ . Each data set is the vector  $\mathbf{x}(t)$  that contains the individual mode frequencies  $Q_{nl}\delta\nu_{nl}/\nu_{nl}$ . These data can be represented as a linear combination of the the eigenvectors with coefficients given by  $c_i(t) = \sum_j \xi_{ij}x_j(t)$  (see the Appendix). The scaled eigenvector  $c_i(t)\xi_i$ , therefore, has a physically reasonable magnitude, and in all following cases, it is this quantity that we invert. In general, we choose the coefficient with the largest magnitude, which represents the largest variation in sound speed. This coefficient is usually the one associated with the set at maximum activity.

### 3. RESULTS & DISCUSSION

#### 3.1. Mean frequencies

We have performed the PCA decomposition of the MDI mean frequencies with respect to the first set (set #1216, start day 1996 May 1, end day 1996 July 12). This is a low activity set. The first four eigenvectors  $\xi_1 - \xi_4$  are shown in Fig. 1, both as a function of frequency and of the lower turning point of the modes. The scaling coefficients for the first four eigenvectors are presented in Fig. 2. Also shown in the figure is the difference in the 10.7 cm radio flux between the first set and the subsequent sets.

When plotted as a function of frequency, the first eigenvector  $\xi_1$  appears to be almost entirely due to near-surface effects — it seems to be a slowly varying function of frequency only. As a function of  $r_t$ , however, a change in the average level of the frequency differences can be seen below the base of the convection zone (around  $r \approx 0.713R_\odot$  — marked by a vertical line in Fig. 1). This implies a time dependent change near the base of the solar convection zone. We conclude, therefore, that there is a statistically significant component of the frequency variability picked out by  $\xi_1$  that does not originate at the surface. The coefficients for  $\xi_1$  are tightly correlated with the 10.7cm radio flux, a proxy for surface activity; the correlation coefficient is 0.99. A linear regression fit to the change in radio flux relative to solar minimum,  $\Delta F_{10.7}$ , gives the relation between the 10.7cm flux and the

coefficients of  $\xi_1$  as:

$$c_1 = (2.53 \times 10^{-5} \pm 3.13 \times 10^{-6})\Delta F_{10.7} + 3.95 \times 10^{-5} \pm 1.6 \times 10^{-4}. \quad (4)$$

Thus, all changes, as manifest by  $\xi_1$ , are tightly correlated with surface magnetic activity.

The second eigenvector,  $\xi_2$ , also shows variability over the solar cycle. Comparing it as a function of  $\nu$  and of  $r_t$ , it is clear that the structure is neither a pure function of frequency nor of lower turning point. The first four obvious downturn features correspond to modes of order  $n = 2, 3, 4$ , and  $5$ . As a function of  $r_t$ , it seems clear that the structure is concentrated at or near the surface. However, the differences can not be fit by the usual “surface term”, and further examination reveals that it cannot be fit even by higher-order surface terms of the form considered in Brodsky & Vorontsov (1993) and Antia (1995). The coefficients for  $\xi_2$  offer some hint as to what is going on. They exhibit no obvious solar cycle dependency, but rather seem to be a roughly linearly decreasing function of time. There does not seem to be any periodicity on a scale of eleven years or shorter. Larson & Schou (2008) have undertaken an in depth study of the systematics in the MDI data reduction pipeline. The plate scale in the MDI instrument has changed slightly over the course of SOHO’s mission, and they have shown that the effect of the resultant error in the measured radius introduces errors that look exactly like the  $\xi_2$  eigenvector computed in this work. We do not believe, therefore, that the features in  $\xi_2$  are solar in origin, but are rather artifacts from the MDI data reduction pipeline. As we will show below, analysis of GONG data confirms our belief.

The third and fourth eigenvectors,  $\xi_3$  and  $\xi_4$  do not exhibit any significant structure at all. The vector  $\xi_3$  shows a slight trend with frequency, but the scaling coefficients  $c_3$  are normally distributed, and we cannot identify any physical significance in this eigenvector. The remaining eigenvectors are statistically consistent with Gaussian noise distributed around zero. We conclude, therefore, that the temporal variation of the MDI frequencies is dependent on a linear combination of  $\xi_1$  and  $\xi_2$  alone. In Fig. 3, we show two data sets reconstructed from the first two eigenvectors. This figure shows that the PCA decomposition does indeed accurately capture the original data while significantly reducing the random scatter in the data. The residuals normalized by the errors are plotted, and are consistent with Gaussian noise, with distributions of  $1.1\sigma$  and  $0.9\sigma$  for the two cases. Having confirmed that the third and subsequent eigenvectors are Gaussian noise, we do not consider them further in this paper. This reduction in noise is important for attempting to invert the small signatures we are looking at here.

The fact that the PCA is applied to a set of mode sets relative to a single base set raises the possibility that we are unduly influenced by the choice of that base set. We therefore repeat the PCA taking a base set from halfway up the solar cycle: MDI set #2224 (start date: 1999 February 3, end date 1999 April 16, and an activity level during the 72 day period



of  $F_{10.7} = 130.7$  SFU). The eigenvectors are consistent with those obtained from the base #1216 set insofar as their inner products are close to unity. We conclude, therefore, that the PCA results are not unduly influenced by the choice of base set.

The mode parameters measured from GONG data are somewhat noisier than those measured from MDI data. Nevertheless, a similar analysis of the GONG data allows us to confirm results obtained from MDI data. The first two eigenvectors from the GONG observations are shown in Fig. 4. As with the MDI data,  $\xi_1$  plotted against  $r_t$  shows some structure in the deep interior. The second eigenvector,  $\xi_2$ , shows no more structure than the MDI  $\xi_3$  eigenvector, and the remaining eigenvectors appear to be Gaussian noise, reinforcing our conclusions that the structure in  $\xi_2$  from the MDI data set is instrumental in origin.

We invert the appropriately scaled  $\xi_1$  eigenvectors to determine the change in the sound speed as a function of radius. We show the results of the inversion of the  $\xi_1$  vector with the #1216 base set in Fig. 5. This vector has been scaled by the coefficient for set #3160 (start date: 2001 August 27) in order to give the inversion results physical meaning. It is readily apparent that at a depth of  $r \approx 0.713R_\odot$ , near the location of the convection zone base, there is a change in the sound speed. This feature is well matched in both the RLS and the SOLA inversions, which implies that the feature is actually present in the data. The depression in sound speed at the base of the convection zone with increasing activity is matched with a corresponding enhancement below the convection zone. We invert the GONG data as well. The inversion results are shown in Fig. 5. There is a clear feature at the base of the convection zone, as seen with MDI data. The presence of this feature in the data of an independent instrument with an independent reduction pipeline is very encouraging — it strongly implies that the changes implied by the inversions are present in the Sun itself rather than artifacts in the data. Figure 5 shows the difference in sound speed between two extrema in the solar cycle. To show how the interior changes with time, in Fig. 6 we show the sound speed inversions at three radii as a function of  $\Delta F_{10.7}$ .

We confirm, therefore, that the signature in mode frequencies is consistent with a change in structure at the base of the convection zone. Other authors have looked for changes in this region, but have not found any changes. The change that we have detected, while statistically significant, is very small, and it is only with the benefit of an entire solar cycle’s worth of high precision observations that we can detect changes at this level. Basu & Antia (2001) examined the mode frequencies for evidence of a change in the location of the base of the convection zone. They did not detect any change, and the sound speed profile that we find in Fig. 5 is very different from the one they expected from a change in the base of the convection zone. This implies that, even if the change we are detecting is thermal in nature, it is unlikely to be related in any way to a change in the position of the base of the

convection zone.

These inversions have been done assuming that the frequency differences are a result of a change in sound speed only. It is almost certain, however, given how tightly correlated this change is with solar activity, that the observed changes are related in some way to changes in the internal magnetic fields. What we have really inverted for, therefore, is a change in the *wave* speed. If we assume that the entire change is due to a change in the wave propagation speed due the presence of magnetic fields, in other words that  $\delta c^2/c^2 \approx v_A^2/c^2$ , as in Basu et al. (2004), we can obtain a value for  $B$ . The change at the base of the convection zone is  $\delta c^2/c^2 = (7.23 \pm 2.08) \times 10^{-5}$ , which implies a magnetic field strength of 290 kG. This is consistent with the results of earlier authors — Goode & Dziembowski (1993) placed an upper limit of 1MG on the toroidal field at the base of the convection zone, and Basu (1997) found that the magnetic field in this region could not exceed 300kG. Chou & Serebryanskiy (2002) found somewhat stronger fields (400 to 700kG).

### 3.2. Latitudinal changes

The MDI and GONG data sets also contain splitting coefficients. The even-order coefficients contain information about the non-spherically symmetric structure in the solar interior. Because the surface manifestations of solar activity are strongly latitudinally dependent, we have used these coefficients to study the temporal variability of structure at different latitudes. The frequencies corresponding to different latitudes are computed using equation 2. The PCA procedure is performed for each latitude as was done with the mean frequencies, and as usual is done with respect to set #1216. The first eigenvector for six different latitudes is shown in Fig. 7. When plotted as a function of frequency, the latitudes from the equator to  $30^\circ$  show a similar frequency dependence as in the case of the mean frequencies in Fig. 1. When plotted as a function of  $r_t$ , we see change at and below the convection zone base. The higher latitudes show no structure, and the eigenvectors for these latitudes are consistent with Gaussian noise. The scaling coefficients for each latitude as a function of time are shown in Fig. 8, along with the surface magnetic field. Like the scaling coefficients for the mean frequencies shown in Fig. 2, the latitudinal scaling coefficients closely follow the surface activity.

We show the sound speed inversions for the equator,  $15^\circ$ ,  $30^\circ$ , and  $45^\circ$  in Fig. 9. The errors in the eigenvectors are larger here than for the mean frequencies, in large part because each frequency is a combination of mean frequency and splitting coefficients, each with their own errors. Nevertheless, there are several points of interest in these inversions. The first is a clear sound speed change for radii greater than approximately  $r = 0.86R_\odot$

at  $15^\circ$  and the equator. The change seen in the SOLA inversion results is well matched in this region by the RLS inversion results, and the significance of the change approaches  $2\sigma$ . There is the possibility, though less statistically significant, of a change at greater depth, i.e., approximately  $r = 0.82R_\odot$ . At  $30^\circ$ , a change in sound speed through the tachocline is seen in the RLS results, but it does not appear to be as clear in the SOLA results. It is unclear whether or not this result is statistically significant. At latitudes of  $45^\circ$  and higher, the inversion errors become large, and the inversion results themselves become extremely sensitive to the inversion parameters. We conclude that there are no structural changes in the solar interior at or above a latitude of  $45^\circ$  large enough to be present in our data sets.

We have also analyzed directly the change in solar structural asphericity over the course of the solar cycle, by taking the scaled frequency differences of high latitudes with respect to the equator. For this analysis, therefore, we have 54 mode sets at each latitude. The difference is equator–latitude. Figure 10 shows the  $\xi_1$  eigenvectors for five different latitudes with respect to the equator. Clearly, the signal to noise in these data are worse than either the latitudinal frequencies or the mean frequencies, but radial structure is discernible in the eigenvectors for the equator relative to  $15^\circ$ ,  $30^\circ$ , and  $45^\circ$ . In fig. 11, the scaling coefficients for the asphericity terms are shown. There is an evident phase delay in the scaling coefficients of  $15^\circ$  and  $30^\circ$  with respect to the equator. This is expected from Fig. 8. The scaling coefficients for higher latitudes ( $45^\circ$  and  $60^\circ$  with respect to the equator) show no structure except for an abrupt change from mostly positive to negative, corresponding closely to the peak of the solar activity cycle.

#### 4. CONCLUSIONS

We have analyzed the changes in solar oscillation frequencies over the course of solar cycle 23. In order to reduce the effects of measurement errors and detect the faintest signatures of solar variability possible, we have employed a Principal Component Analysis of the frequencies. The mean frequencies are known to vary over the solar cycle, and this variation is known to be tightly correlated with surface activity. We have found this correlation as well.

In addition to the frequency dependent change which these earlier authors have detected, we have found a small but statistically significant change in modes with turning points at or below the convection zone. This confirms the result of Chou & Serebryanskiy (2005). This signature is present in both the MDI and the GONG data sets. We have inverted these results to obtain the difference in sound speed, and we have confirmed that there is a change in solar structure at the base of the convection zone over the course of the solar cycle. The

measured change at a radius of  $r = (0.712_{-0.0029}^{+0.0097})R_{\odot}$  is  $\delta c^2/c^2 = (7.23 \pm 2.08) \times 10^{-5}$ , where the errors in radius are a measure of the resolution of the inversion taken from the first and third quartile points of the inversion kernel.

We have also used the splitting coefficients to investigate how the changes in structure vary over latitude. We have found that the changes in the solar interior are tightly correlated with the latitudinal distribution of surface activity. The most statistically significant changes detected in the analysis are changes in sound speed in the outer ten percent (by radius) of the solar interior.

We wish to thank the anonymous referee for helpful comments which helped to clarify a number of the discussions in this paper. We are also grateful to T. Larson and J. Schou for their helpful discussion of the anomalous results in the MDI data. This work utilizes data obtained by the Global Oscillation Network Group (GONG) project, managed by the National Solar Observatory, which is operated by AURA, Inc. under a cooperative agreement with the National Science Foundation. The data were acquired by instruments operated by the Big Bear Solar Observatory, High Altitude Observatory, Learmonth Solar Observatory, Udaipur Solar Observatory, Instituto de Astrofisico de Canarias, and Cerro Tololo Inter-American Observatory. This work also utilizes data from the Solar Oscillations Investigation/ Michelson Doppler Imager (SOI/MDI) on the Solar and Heliospheric Observatory (SOHO). SOHO is a project of international cooperation between ESA and NASA. MDI is supported by NASA grants NAG5-8878 and NAG5-10483 to Stanford University. This work is partially supported by NSF grants ATM 0348837 and ATM 073770 to SB.

## A. PRINCIPAL COMPONENT ANALYSIS

We give a brief description of the Principal Component Analysis technique that follows the one found in Kendall (1980). This technique assumes that we begin with a set of observations, each one consisting of a set of data points (for example, a set of spectra of different objects, or a set of images, or, as in this paper, sets of mode frequency measurements at different points in time). Assume we have  $m$  observations, each with  $n$  data points. The  $m$  vectors  $\mathbf{x}_i$  each contain the  $n$  data points  $x_{ij}$ , measured relative to the mean  $\bar{\mathbf{x}}_j$ . We wish to find a new set of vectors  $\mathbf{c}_i$  that are linearly dependent on  $\mathbf{x}_i$ , and uncorrelated with each other. In addition, we require that they have stationary values of their variance. This condition is imposed to ensure that most of the variance is accounted for in as few vectors  $\mathbf{c}_i$  as possible. Alternatively, this condition can be viewed geometrically as a rotation of the basis vectors such that the variance of the data with respect to each basis vector is maximal.

This is most easily understood in the case of a two dimensional data set, where PCA is equivalent to a linear fit to the data, and the rotation sets one basis vector parallel to that fit. The vectors  $\mathbf{c}_i$  will be given by a linear combination of the original observations:

$$\mathbf{c}_i = \sum_{j=1}^n \xi_{ji} \mathbf{x}_j. \quad (\text{A1})$$

The vectors  $\boldsymbol{\xi}_j$  will form a new basis set for the observations. The variance of  $\mathbf{c}_i$  is given by

$$\text{var } \mathbf{c}_i = \sum_{j=1}^n \sum_{k=1}^n \xi_{ji} \xi_{ki} e_{jk}, \quad (\text{A2})$$

where  $e_{jk}$  is the covariance between  $x_j$  and  $x_k$ . The covariance matrix is given by

$$\mathbf{E} = \frac{1}{n} \mathbf{X} \mathbf{X}^T, \quad (\text{A3})$$

where  $\mathbf{X}$  is the matrix  $(\mathbf{x}_1, \mathbf{x}_2, \dots, \mathbf{x}_m)$ . In order to get unique solutions for the values of  $\xi_{ji}$ , we impose a normalization condition:

$$\sum_{i=1}^m \xi_{ji}^2 = 1. \quad (\text{A4})$$

Finding the stationary values of  $\text{var } \mathbf{c}_i$  (eq. A2) with the condition A4 is equivalent to finding the stationary values of:

$$\sum_{j=1}^m \sum_{k=1}^m \xi_{ij} \xi_{ik} e_{jk} - \lambda \left( \sum_{j=1}^m \xi_{ij}^2 - 1 \right), \quad (\text{A5})$$

where  $\lambda$  is some constant. To find the stationary values, we differentiate A5 by  $\xi_{ij}$  and find the roots of the equation:

$$\sum_{k=1}^m \xi_{ik} e_{jk} - \lambda \xi_{ij} = 0. \quad (\text{A6})$$

This is an eigenvalue problem — the vector  $\boldsymbol{\xi}_j$  is an eigenvector of  $\mathbf{E}$  and  $\lambda$  is the corresponding eigenvalue. The eigenvectors form an orthonormal basis set and are called the ‘principal components’ of the data set. When they are ordered by decreasing eigenvalue  $\lambda$ , the first principal component will have the largest possible variance, the second the second largest variance, and so on. In our work, we use the singular value decomposition of the covariance matrix to get the eigenvalues and vectors. The vectors  $\mathbf{c}_i$  are the scaling coefficients for the principal components.

The PCA technique has several known weaknesses. The first is that its simplest implementation requires a completely filled covariance matrix — in other words there can be no missing data in  $\mathbf{X}$ . This is a problem for us since not all modes are identified in each different observation epoch. There are generalizations of the technique which allow for large quantities of missing data. In our case, however, the modes in which we are interested tend to be identified in most of the mode sets, so we can simply interpolate the missing modes from the existing frequency measurements without any significant effect on the results. We do not, therefore, use a more specialized technique.

A second problem with PCA is its sensitivity to outliers. One often-quoted example shows a PCA decomposition where the correlation coefficient between the first two components with one outlier removed is 0.99 (e.g., Huber 1981). There are available routines for making PCA more robust, but in our case, because the dimensionality of the problem is relatively small, we can instead empirically test the sensitivity of the data set to outliers. Monte Carlo tests show that our data set is not prone to errors in the PCA due to outliers.

Principal Component Analysis has been used in a wide variety of astronomical contexts (see references in Murtagh & Heck 1987, Chapter2). In solar physics, PCA has been used for, among other things, the inversion of Stokes profiles (e.g., Eydenberg et al. 2005; Rámirez Vélez et al. 2006), in detecting structures in coronal activity (e.g., Cadavid et al. 2007), and in helioseismic rotation inversions (e.g., Eff-Darwich et al. 2004).

## REFERENCES

- Anguera Gubau, M., Palle, P. L., Perez Hernandez, F., Regulo, C., & Roca Cortes, T. 1992, *A&A*, 255, 363
- Antia, H. M. 1995, *MNRAS*, 274, 499
- Antia, H. M., & Basu, S. 1994, *A&AS*, 107, 421
- Antia, H. M., & Basu, S. 2000, *ApJ*, 541, 442
- Antia, H. M., & Basu, S. 2001, *ApJ*, 559, L67
- Antia, H. M., Basu, S., Hill, F., Howe, R., Komm, R. W., & Schou, J. 2001, *SOHO 10/GONG 2000 Workshop: Helio- and Asteroseismology at the Dawn of the Millennium*, 464, 45
- Bachmann, K. T., & Brown, T. M. 1993, *ApJ*, 411, L45
- Balmforth, N. J., Gough, D. O., & Merryfield, W. J. 1996, *MNRAS*, 278, 437

- Basu, S. 1997, MNRAS, 288, 572
- Basu, S. 2002, From Solar Min to Max: Half a Solar Cycle with SOHO, 508, 7
- Basu, S., & Antia, H. M. 2000, Sol. Phys., 192, 449
- Basu, S., & Antia, H. M. 2001, SOHO 10/GONG 2000 Workshop: Helio- and Asteroseismology at the Dawn of the Millennium, 464, 297
- Basu, S., & Antia, H. M. 2006, Proceedings of SOHO 18/GONG 2006/HELAS I, Beyond the spherical Sun, 624, 128
- Basu, S., Antia, H. M., & Bogart, R. S. 2004, ApJ, 610, 1157
- Basu, S., Antia, H. M., & Bogart, R. S. 2007, ApJ, 654, 1146
- Basu, S., & Mandel, A. 2004, ApJ, 617, L155
- Basu, S., & Thompson, M. J. 1996, A&A, 305, 631
- Brodsky, M., & Vorontsov, S. V. 1993, ApJ, 409, 455
- Cadavid, A. C., Lawrence, J. K., & Ruzmaikin, A. 2008, Sol. Phys., 248, 247
- Chaplin, W. J., Elsworth, Y., Isaak, G. R., New, R., & Appourchaux, T. 2001, SOHO 10/GONG 2000 Workshop: Helio- and Asteroseismology at the Dawn of the Millennium, 464, 83
- Charbonneau, P. 2005, Living Reviews in Solar Physics, 2, 2
- Chou, D.-Y., & Serebryanskiy, A. 2002, ApJ, 578, L157
- Chou, D.-Y., & Serebryanskiy, A. 2005, ApJ, 624, 420
- Chou, D.-Y., Serebryanskiy, A., & Sun, M.-T. 2003, Space Science Reviews, 107, 35
- Christensen-Dalsgaard, J. 2002, Reviews of Modern Physics, 74, 1073
- Christensen-Dalsgaard, J., & Berthomieu, G. 1991, Solar Interior and Atmosphere, 401
- Durney, B. R., Hill, F., & Goode, P. R. 1988, ApJ, 326, 486
- Duvall, T. L., Jr., Harvey, J. W., & Pomerantz, M. A. 1986, Nature, 321, 500
- Dziembowski, W. A., & Goode, P. R. 1991, Solar Interior and Atmosphere, 501

- Dziembowski, W. A., & Goode, P. R. 2005, *ApJ*, 625, 548
- Eff-Darwich, A., Korzennik, S. G., Jiménez-Reyes, S., & García, R. A. 2004, *SOHO 14 Helio- and Asteroseismology: Towards a Golden Future*, 559, 420
- Eff-Darwich, A., Korzennik, S. G., Jiménez-Reyes, S. J., & Pérez Hernández, F. 2002, *ApJ*, 580, 574
- Elsworth, Y., Howe, R., Isaak, G. R., McLeod, C. P., Miller, B. A., New, R., Speake, C. C., & Wheeler, S. J. 1994, *ApJ*, 434, 801
- Elsworth, Y., Howe, R., Isaak, G. R., McLeod, C. P., & New, R. 1990, *Nature*, 345, 322
- Eydenberg, M. S., Balasubramaniam, K. S., & López Ariste, A. 2005, *ApJ*, 619, 1167
- Goldreich, P., Murray, N., Willette, G., & Kumar, P. 1991, *ApJ*, 370, 752
- Goode, P. R., & Dziembowski, W. A. 1993, *GONG 1992. Seismic Investigation of the Sun and Stars*, 42, 229
- Gough, D. O. 2002, *From Solar Min to Max: Half a Solar Cycle with SOHO*, 508, 577
- Gough, D. O., & Thompson, M. J. 1990, *MNRAS*, 242, 25
- Hill, F., et al. 1996, *Science*, 272, 1292
- Howe, R., Christensen-Dalsgaard, J., Hill, F., Komm, R. W., Larsen, R. M., Schou, J., Thompson, M. J., & Toomre, J. 2000, *Science*, 287, 2456
- Howe, R., Christensen-Dalsgaard, J., Hill, F., Komm, R., Schou, J., & Thompson, M. J. 2005, *ApJ*, 634, 1405
- Howe, R., Komm, R., & Hill, F. 1999, *ApJ*, 524, 1084
- Howe, R., Komm, R. W., & Hill, F. 2002, *ApJ*, 580, 1172
- Howe, R., Rempel, M., Christensen-Dalsgaard, J., Hill, F., Komm, R., Larsen, R. M., Schou, J., & Thompson, M. J. 2006, *ApJ*, 649, 1155
- Huber, P. J., 1981, *Robust Statistics*, (New York, NY: Wiley)
- Kendall, M. 1980, *Multivariate Analysis*, (2nd Ed.; New York, NY: Macmillan Publishing Co)
- Korzennik, S. G., Rabello-Soares, M. C., & Schou, J. 2004, *ApJ*, 602, 481



- Kuhn, J. R. 1988, *ApJ*, 331, L131
- Larson, T., & Schou, J. 2008, in *Helioseismology, Asteroseismology and MHD Connections*, J. Phys.: Conf. Ser., ed. Gizon, L., in press
- Li, L. H., Basu, S., Sofia, S., Robinson, F. J., Demarque, P., & Guenther, D. B. 2003, *ApJ*, 591, 1267
- Libbrecht, K. G., & Woodard, M. F. 1990, *Nature*, 345, 779
- Murtagh, F., & Heck, A. 1987, *Astrophysics and Space Science Library*, 131
- Pijpers, F. P., & Thompson, M. J. 1994, *A&A*, 281, 231
- Rabello-Soares, M. C., Basu, S., & Christensen-Dalsgaard, J. 1999, *MNRAS*, 309, 35
- Rabello-Soares, M. C., Korzennik, S. G., & Schou, J. 2001, *SOHO 10/GONG 2000 Workshop: Helio- and Asteroseismology at the Dawn of the Millennium*, 464, 129
- Rámirez Vélez, J. C., Semel, M., Stift, M. J., & Leone, F. 2006, *Astronomical Society of the Pacific Conference Series*, 358, 405
- Regulo, C., Jimenez, A., Palle, P. L., Perez Hernandez, F., & Roca Cortes, T. 1994, *ApJ*, 434, 384
- Rhodes, E. J., Jr., Reiter, J., Kosovichev, A. G., Schou, J., & Scherrer, P. H. 1998, *Structure and Dynamics of the Interior of the Sun and Sun-like Stars*, 418, 73
- Ritzwoller, M. H., & Lavelly, E. M. 1991, *ApJ*, 369, 557
- Schou, J. 1999, *ApJ*, 523, L181
- Sekii, T. 1997, *Sounding Solar and Stellar Interiors*, 181, 189
- Serebryanskiy, A., & Chou, D.-Y. 2005, *ApJ*, 633, 1187
- Tapping, K. F. 1987, *J. Geophys. Res.*, 92, 829
- Verner, G. A., Chaplin, W. J., & Elsworth, Y. 2004, *MNRAS*, 351, 311
- Verner, G. A., Chaplin, W. J., & Elsworth, Y. 2006, *ApJ*, 640, L95
- Woodard, M. F., & Noyes, R. W. 1985, *Nature*, 318, 449
- Woodard, M. F., Libbrecht, K. G., Kuhn, J. R., & Murray, N. 1991, *ApJ*, 373, L81

Vorontsov, S. V., Christensen-Dalsgaard, J., Schou, J., Strakhov, V. N., & Thompson, M. J.  
2002, *Science*, 296, 101

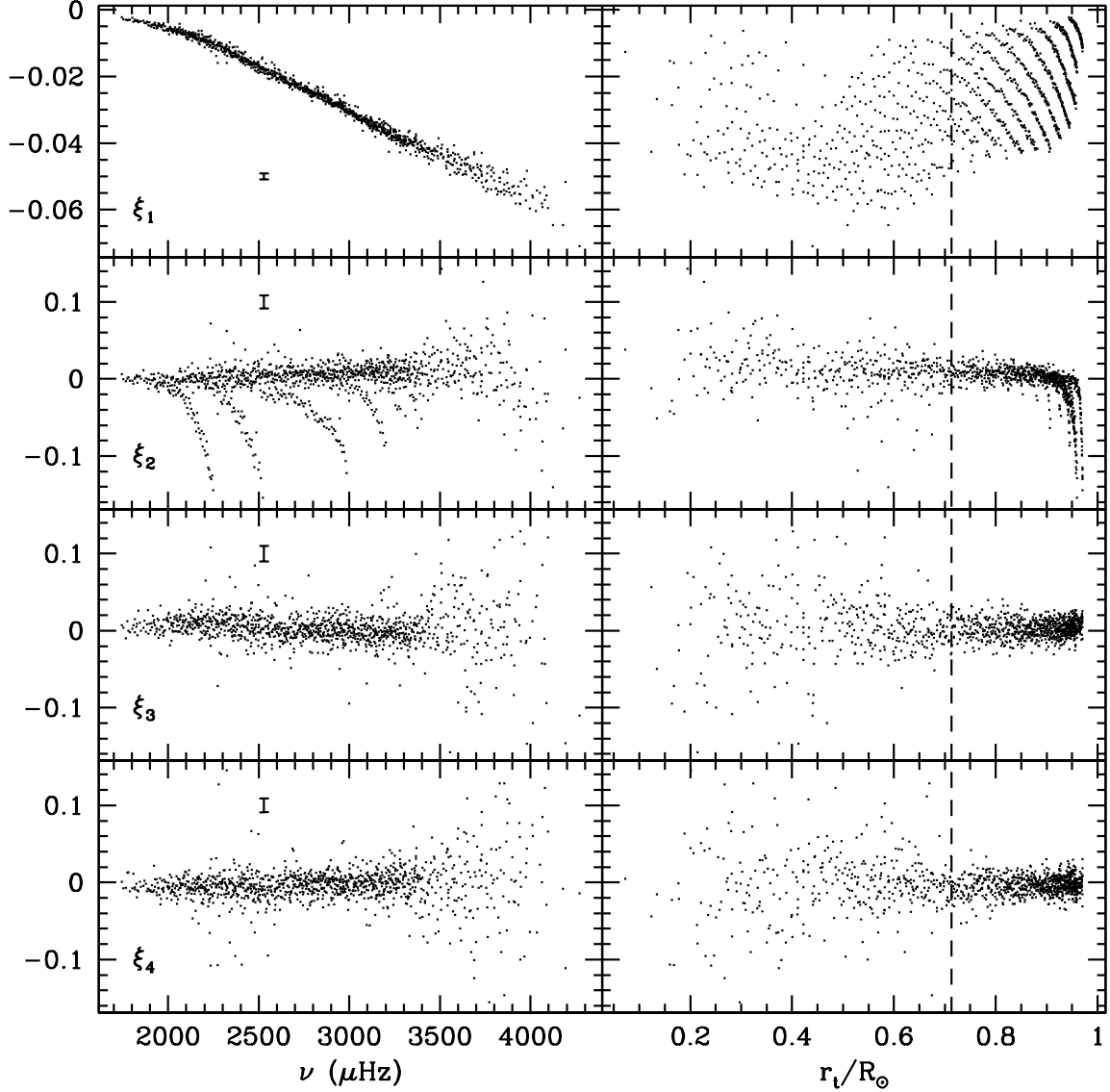


Fig. 1.— The first four eigenvectors for the MDI data set are shown. The base set is #1216 (1996 May 1). The left-hand panels show the eigenvectors as a function of frequency, and the right-hand panels show it as a function of the lower turning point of the mode. The vertical line shows the position of the base of the convection zone. The vertical axis units are arbitrary (the vectors are normalized so that  $\xi_i \cdot \xi_i = 1$ ). The error bars show representative errors calculated using a Monte Carlo simulation.

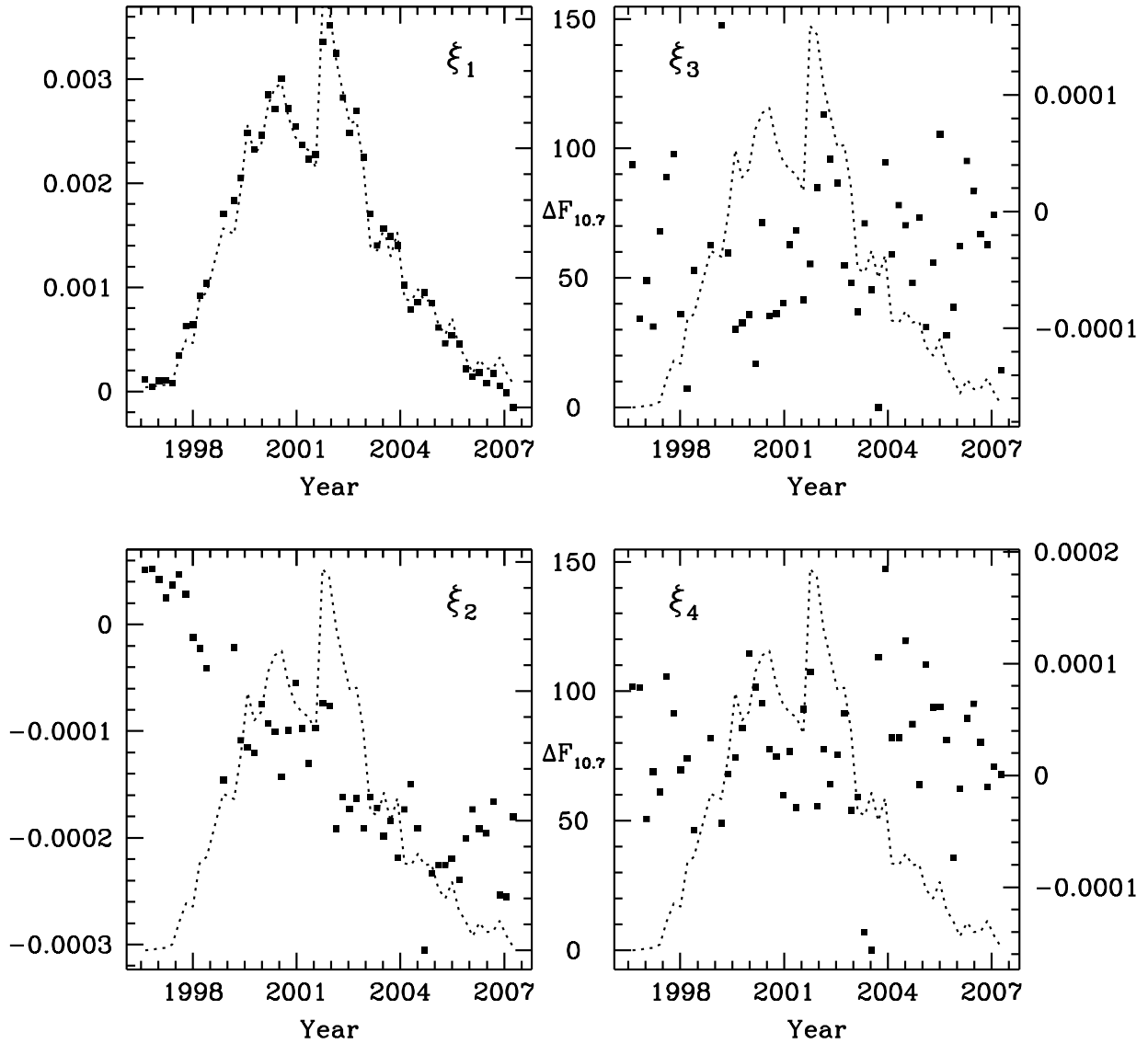


Fig. 2.— The scaling coefficients for the first four eigenvectors are shown as points. They are shown as a function of time (the start date of the MDI mode sets). The dotted line is the change in 10.7cm radio flux with respect to the beginning of the solar cycle. The units are Solar Flux Units (SFU).

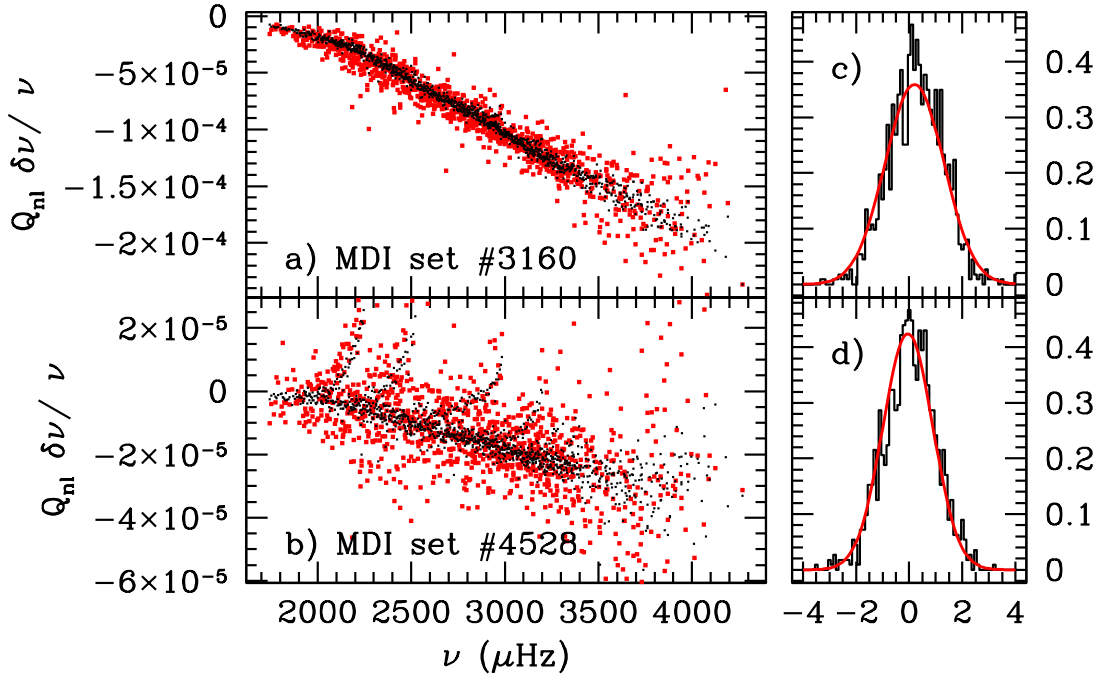


Fig. 3.— To demonstrate that the PCA representation of the data does indeed capture the actual data, we present two reconstructed data sets and compare them to the actual data. Two frequency difference sets are examined: sets #3160 (2001 August 27, panel a) and # 4528 (2005 May 26, panel b), both with respect to # 1216. At left, the frequency differences are plotted (panel (c) for set #3160 and panel (d) for set #4528). The actual data is shown in red, and the reconstructed data set using  $\xi_1$  and  $\xi_2$  are overplotted in black. The normalized residuals are binned and shown against a Gaussian curve to show that the information which has been removed is statistically random.

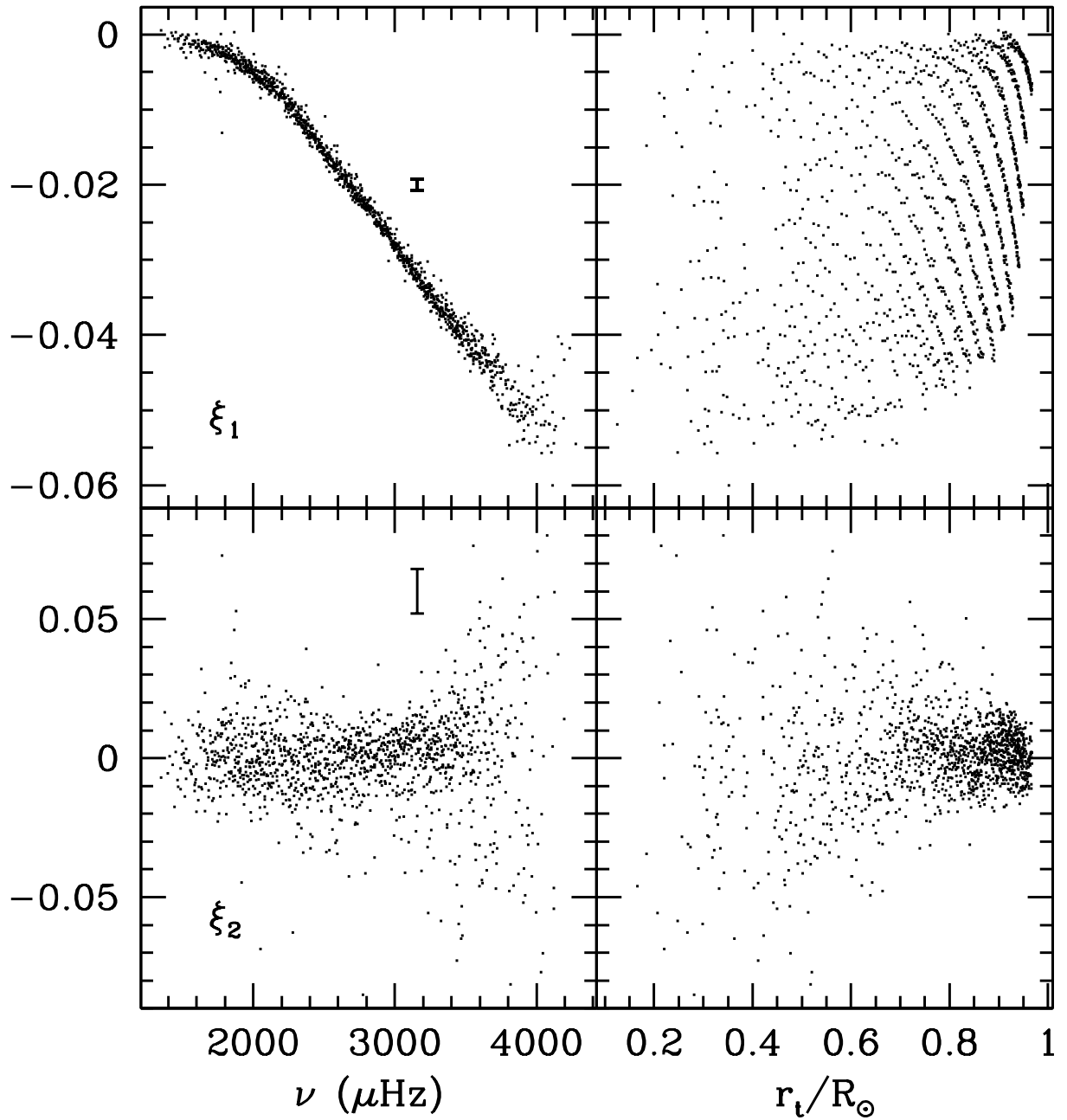


Fig. 4.— The first two eigenvectors for the GONG data sets plotted as a function of frequency (the left-hand panels) and as a function of the lower turning radius (the right-hand panels). The first eigenvector  $\xi_1$  shows a signature similar to the one seen in the MDI data, albeit much less obviously. The eigenvector  $\xi_2$  shows no structure, unlike the equivalent eigenvector for MDI, implying that the MDI  $\xi_2$  is an instrumental artifact.

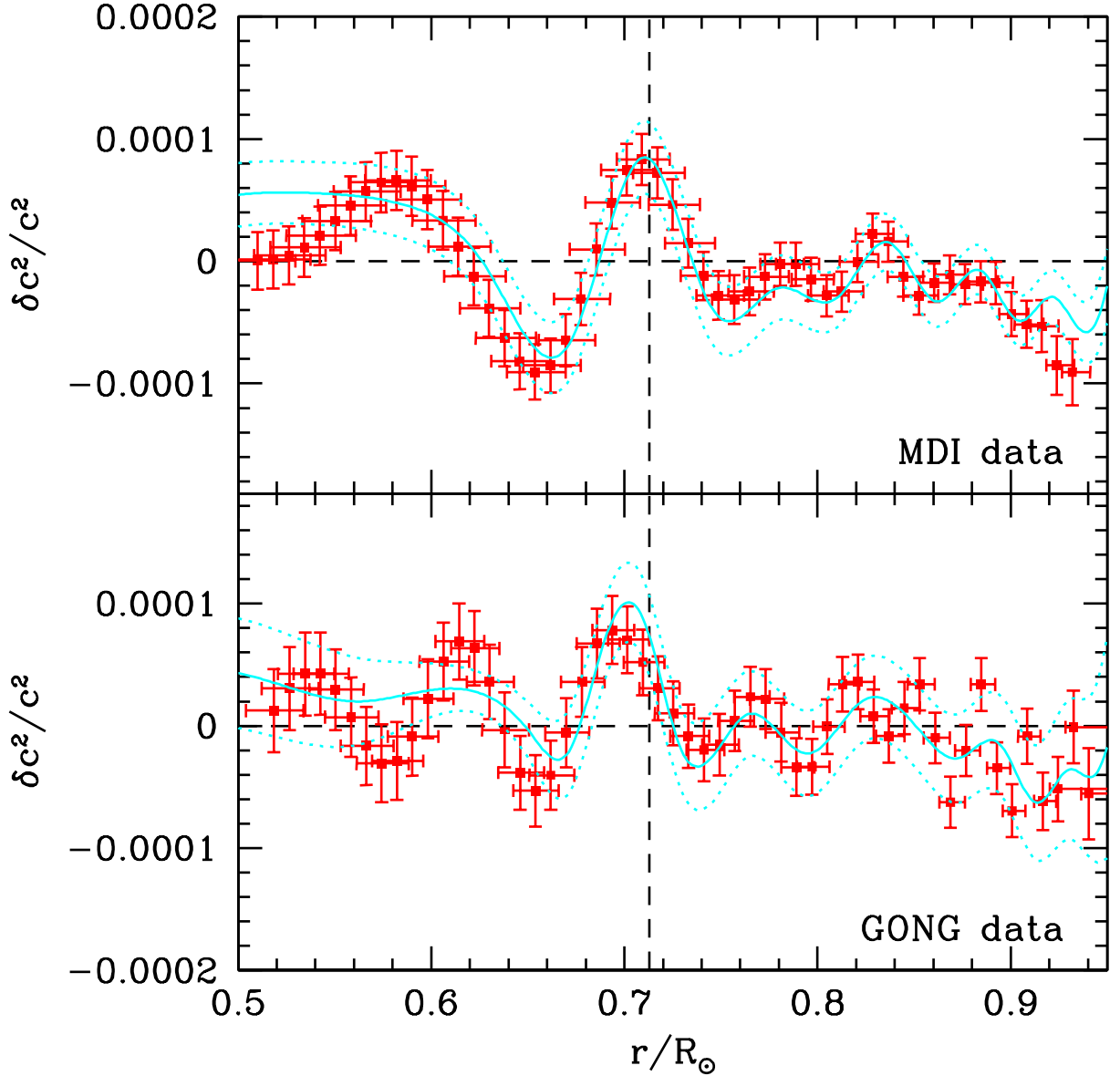


Fig. 5.— Inversion for sound speed of the  $\xi_1$  eigenvector. The top panel shows the inversion of the MDI data. The lower panel shows the inversion of the GONG data. The solid cyan line is the result from the RLS inversion (the dotted lines are the vertical error bounds). The red points are the results from the SOLA inversion. The horizontal dashed line is the zero-point. The vertical dashed line represents the location of the base of the convection zone. At the convection zone base, the MDI inversion results show a clear depression in sound speed at high activity (the sense of the inversion is low activity minus high activity) and an enhancement in the tachocline region. The depression is matched in the GONG inversion results. The location of this feature, though slightly deeper, is within the horizontal errors of the MDI result.

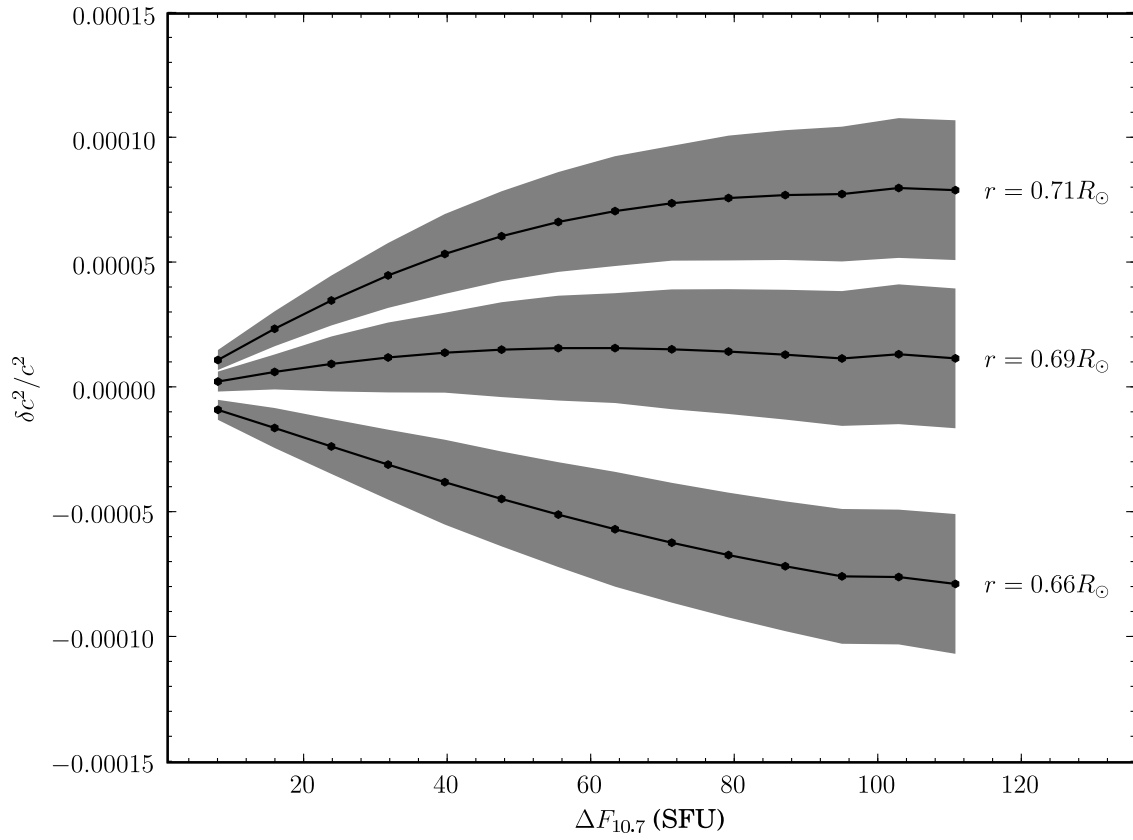


Fig. 6.— Change in inferred sound speed as function of activity level (10.7cm radio flux) is shown for different radii around the base of the convection zone. The shaded regions show the errors for each set of inversions.



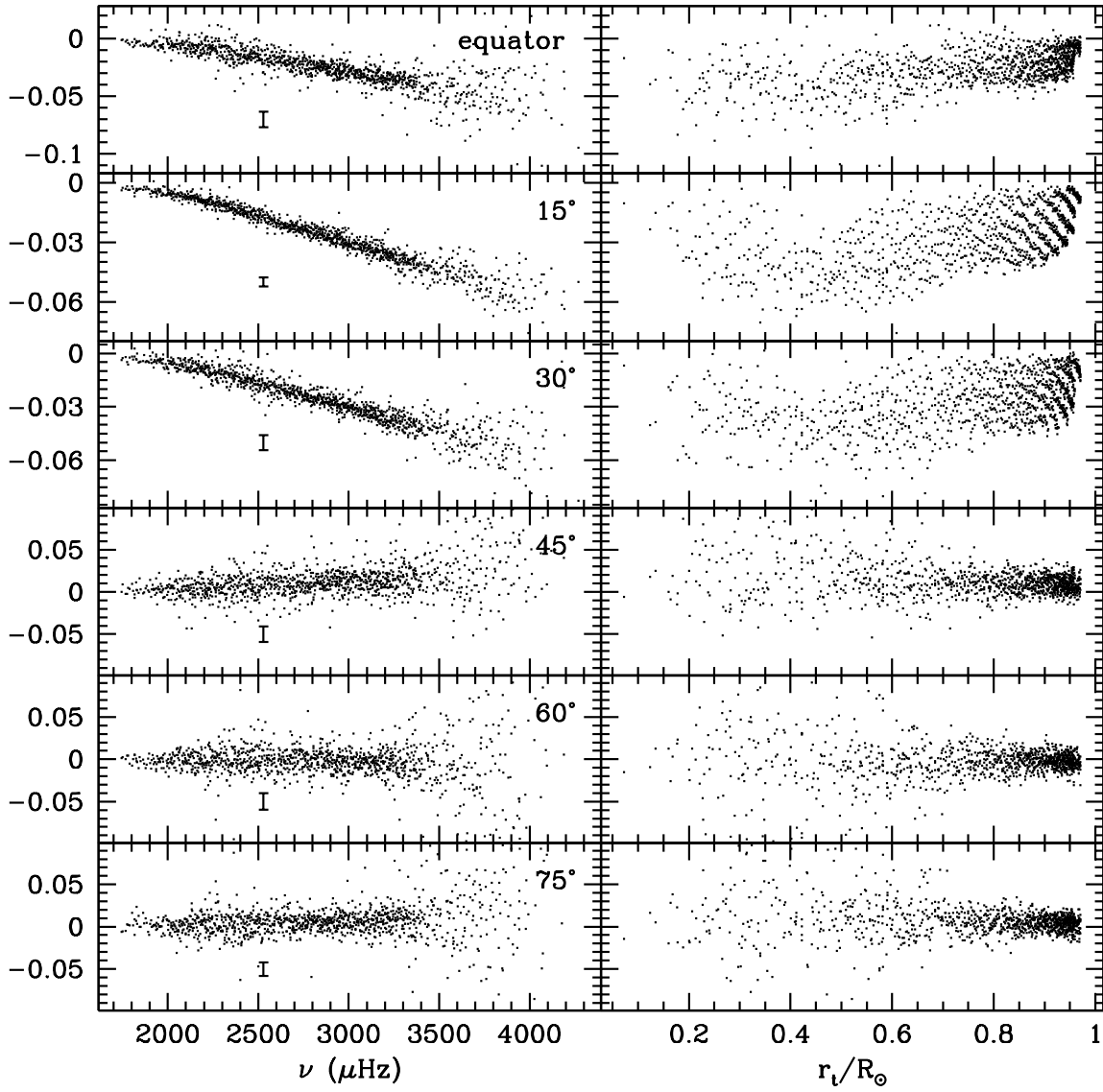


Fig. 7.— The first eigenvector  $\xi_1(\theta)$  for latitudes from  $0^\circ$  to  $75^\circ$ . The data are from MDI and are relative to the #1216 mode set. The left-hand panels show the eigenvectors as functions of frequency, and the right-hand panels as functions of the lower turning points.

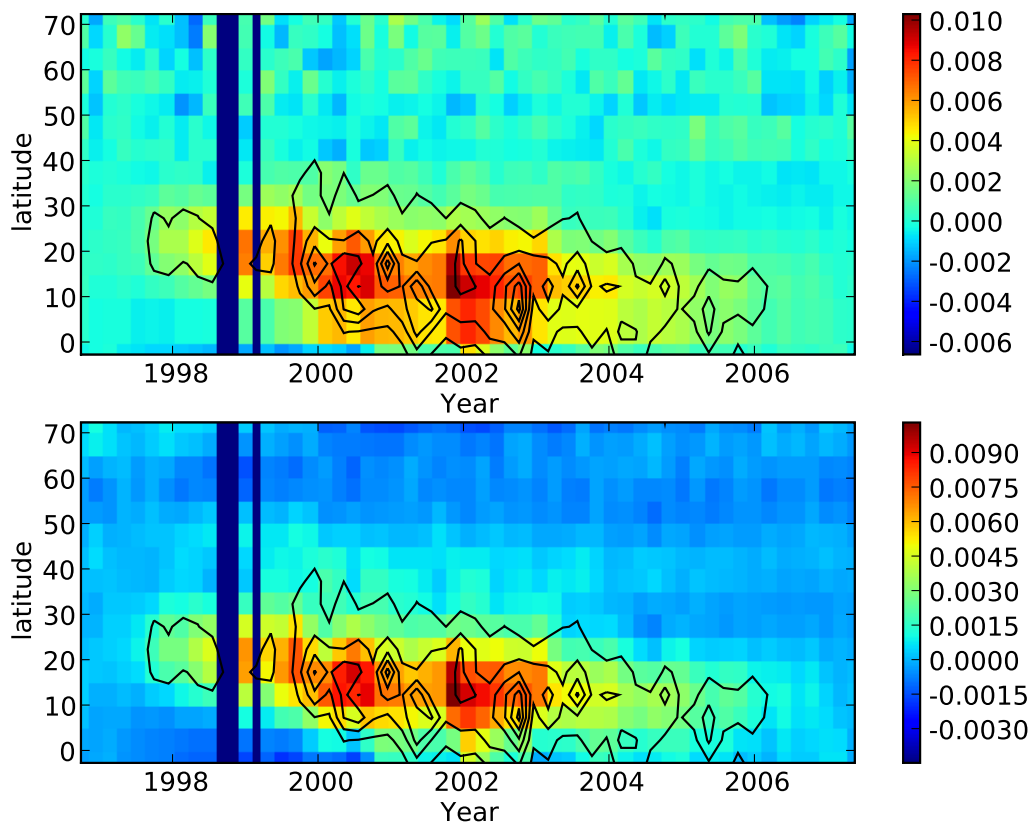


Fig. 8.— The scaling coefficients are plotted as a function of time and latitude. The top panel shows the coefficients for each individual eigenvector  $\xi_1(\theta)$ . The bottom panel shows the scaling coefficients for all the latitudes as a function of the  $\xi_1(15^\circ)$ . This shows how the changes represented by that eigenvector change as a function of both time and latitude. The average unsigned magnetic flux from MDI carrington rotation synoptic maps over each 72-day period is shown in contour. The contours are spaced every 52G, with the lowest at 56.5G. The vertical bars in 1998 are gaps in MDI coverage due to spacecraft problems.

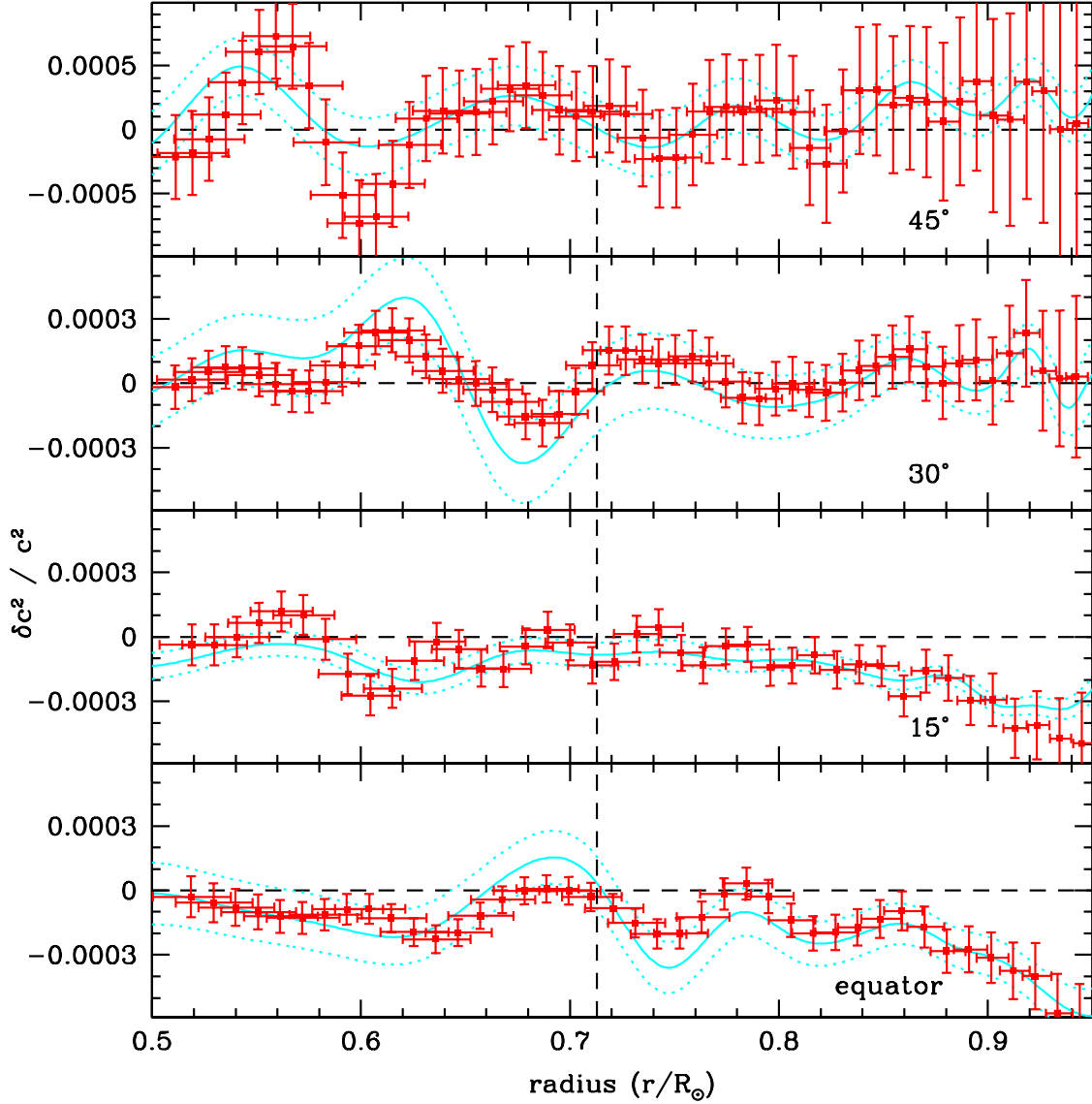


Fig. 9.— The inversions of the latitudinal frequencies are shown for four different latitudes from the equator to  $45^\circ$ . The differences are with respect to MDI set #1216. As expected from an examination of the raw frequencies, there are no discernible features in the inversion for  $45^\circ$  and above — the inversions are extremely unstable to the choice of inversion parameters. At  $15^\circ$  and the equator, a significant (about  $2\sigma$ ) enhancement in sound speed at high activity is observed above approximately  $r = 0.98R_\odot$ . As before, the vertical dashed line indicates the position of the base of the convection zone ( $r = 0.713R_\odot$ ).

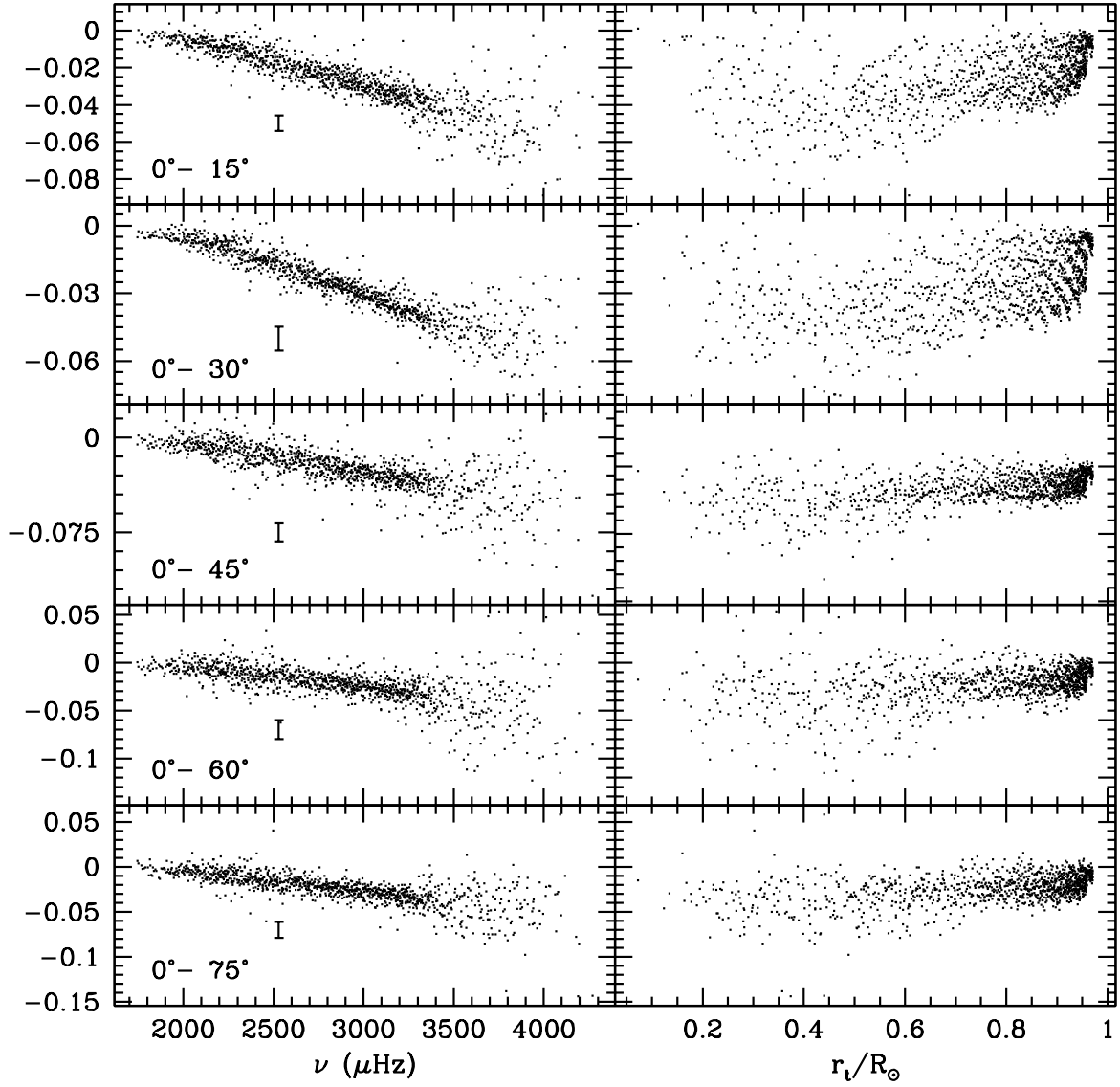


Fig. 10.— The  $\xi_1$  eigenvectors for the asphericity terms — equator minus latitude — are shown for five different latitudes. As usual, the left panels show the eigenvectors with respect to frequency, and the right hand panels are with respect to lower turning point.

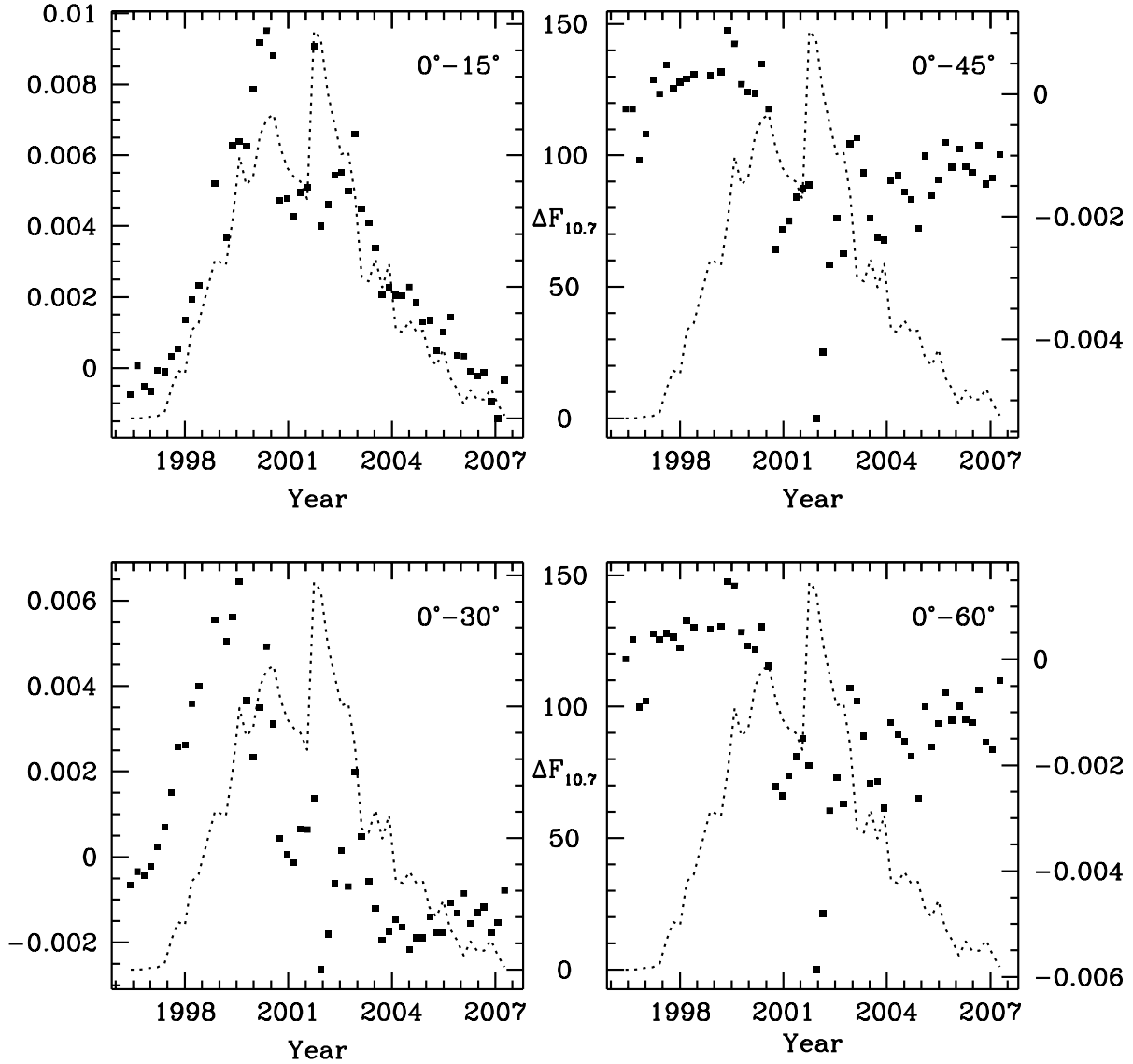


Fig. 11.— The scaling coefficients for the asphericity eigenvectors are shown. The dotted line is the  $F_{10.7}$  flux. The  $0^\circ - 15^\circ$  and  $0^\circ - 30^\circ$  both show a phase shift, consistent with the butterfly diagram from Fig. 8. The higher latitudes show a distinct change from mostly positive to negative at high activity.